The IAA cosmic dust laboratory: Experimental scattering matrices of clay particles

O. Muñoz [a,*], F. Moreno [a], D. Guirado [a], J.L. Ramos [a], H. Volten [b], J.W. Hovenier [c]

[a] Instituto de Astrofísica de Andalucía, CSIC, Glorieta de la Astronomía sn, 18080 Granada, Spain
[b] Netherlands National Institute for Public Health and the Environment, Centre for Environmental Monitoring, P.O. Box 1, NL 3720 BA Bilthoven, The Netherlands
[c] Astronomical Institute "Anton Pannekoek", University of Amsterdam, P.O. Box 94249, 1090 GE Amsterdam, The Netherlands

ABSTRACT

We present the first results of measurements on solid particles performed at the Instituto de Astrofísica de Andalucía (IAA) cosmic dust laboratory located in Granada, Spain. The laboratory apparatus measures the complete scattering matrix as a function of the scattering angle of aerosol particles. The measurements can be performed at a wavelength (λ) of 483, 488, 520, 568, or 647 nm in the scattering angle range from 3° to 177°. Results of special test experiments are presented which show that our experimental results for scattering matrices are not significantly contaminated by multiple scattering and that the sizes/shapes of the particles do not change during the measurements. Moreover, the measured scattering matrix for a sample of green clay particles is compared with measurements previously performed in the Amsterdam light scattering setup for the same sample. New measurements on a white clay sample at 488 and 647 nm are also presented. The apparatus is devoted to experimentally studying the angle dependence of scattering matrices of dust samples of astrophysical interest. Moreover, there is a great interest in similar studies of aerosols that can affect the radiative balance of the atmosphere of the Earth and other planets such as silicates, desert dust, volcanic ashes, and carbon soot particles.

© 2010 Elsevier Inc. All rights reserved.

1. Introduction

Irregular mineral particles play an important role in the radiative balance of planetary and minor bodies atmospheres in the Solar System (see e.g. Hovenier and Muñoz, 2009). These mineral particles seem to occur with a broad range of shapes and to be distributed in size from the sub-micron region up to millimeters (e.g. d'Almeida et al., 1991; Muñoz et al., 1999; Fulle, 2004; Wolff et al., 2006). The scattering properties of this kind of dust particles are an important diagnostic tool which contains essential information about the nature of the grains. Light scattering properties of homogeneous spherical particles can be easily computed from Lorenz–Mie theory without any restriction about the size or refractive index of the particles. However, although remarkable progress in developing advanced numerical algorithms for computing electromagnetic scattering by nonspherical particles has been achieved during the last decades (e.g. Mishchenko et al., 1996, 2000; Draine and Flatau, 2003; Kahnert, 2003; Taflove and Hagness, 2005; Yurkin and Hoekstra, 2007; Muinonen et al., 2009; Wriedt, 2009, see also http://www.scattport.org), an exact solution for realistic polydispersions of irregular dust particles is still far from trivial. In most cases computations for realistic polydisperse irregular particles have to be replaced by computations for simplified models.

Consequently, laboratory measurements remain an indispensable tool for testing the reliability of scattering calculations for model particles (see e.g. Mishchenko et al., 1997; Nousiainen et al., 2006; Vilaplana et al., 2004; Min et al., 2005; Moreno et al., 2007; Zubko et al., 2009.)

In the last decades, the experimental setup located in Amsterdam, The Netherlands (Hovenier, 2000), has produced a significant amount of experimental data that are freely available in digital form in the Amsterdam Light Scattering Database at http://www.astro.uva.nl/scatter (Volten et al., 2005, 2006). Unfortunately, the Dutch setup was closed in 2007. An improved descendant of the Dutch experimental setup has been recently constructed at the Instituto de Astrofísica de Andalucía, CSIC. Hereafter we will call this the IAA cosmic dust laboratory. For a detailed description of the experimental apparatus and data reduction process we refer to Muñoz et al. (2010).

In this work we present the first measurements with solid particles performed at the IAA cosmic dust laboratory. The measurements have been performed on a sample of randomly oriented white clay particles. Clay is believed to occur on different Solar System bodies such as Mars with considerable abundances in the form of dust particles, both on the surface and in the atmosphere (Clancy et al., 1995; Bandfield, 2002), and satellites and asteroids (Webster, 1988; Starukhina and Shkuratov, 1997; Bland et al., 2000). Moreover, it is an important component of mineral aerosols in the Earth atmosphere (e.g. Sokolik and Toon, 1999; Nousiainen, 2009; Matsuki et al., 2010). Several issues relevant to the reliability

---

* Corresponding author. Fax: +34 958 814530.
   E-mail address: olga@iaa.es (O. Muñoz).

of the experimental data obtained for dust particles are also discussed.

A review of the theory involved in these experiments is presented in Section 2. In Section 3, we give a brief description of the IAA cosmic dust laboratory. Various tests regarding the reliability of the data are also presented. In Section 4 we describe the physical properties of the clay sample together with the measured scattering matrices. Future work is discussed in Section 5.

2. The scattering matrix

The flux and state of linear and circular polarization of a quasi-monochromatic beam of light can be described by means of the so-called flux vector whose elements are Stokes parameters (Van de Hulst, 1957; Hovenier et al., 2004). If such a beam of light is scattered by an ensemble of particles separated by distances much larger than their linear dimensions and in the absence of multiple scattering, the flux vectors of the incident beam $\pi\mathbf{\Phi}_0$ and scattered beam $\pi\mathbf{\Phi}_{det}$ are, for each scattering direction, related by the so called scattering matrix, as follows (Van de Hulst, 1957; Hovenier et al., 2004):

$$\mathbf{\Phi}_{det} = \frac{\lambda^2}{4\pi^2 D^2} \begin{pmatrix} F_{11} & F_{12} & F_{13} & F_{14} \\ F_{21} & F_{22} & F_{23} & F_{24} \\ F_{31} & F_{32} & F_{33} & F_{34} \\ F_{41} & F_{42} & F_{43} & F_{44} \end{pmatrix} \mathbf{\Phi}_0. \quad (1)$$

Here the first elements of the column vectors are fluxes divided by π and the other elements describe the state of polarization of the beams. Furthermore, λ is the wavelength of the incident light, and D is the distance between the ensemble of particles and the detector. The 16 elements of the scattering matrix, $F_{i,j}$, with $i, j = 1$–4, are dimensionless, and depend on the number and physical properties of the particles (size, shape, structure, and refractive index), orientation of the particles, the wavelength of the incident light, and the directions of incidence and scattering. For randomly oriented particles, all scattering planes are equivalent. Thus, the scattering direction is fully described by the scattering angle θ, i.e. the angle between the directions of propagation of the incident and the scattered beams.

When randomly oriented particles and their mirror particles are present in equal numbers in the ensemble, the scattering matrix has the simple form (see e.g. Van de Hulst, 1957):

$$\mathbf{\Phi}_{det} = \frac{\lambda^2}{4\pi^2 D^2} \begin{pmatrix} F_{11} & F_{12} & 0 & 0 \\ F_{12} & F_{22} & 0 & 0 \\ 0 & 0 & F_{33} & F_{34} \\ 0 & 0 & -F_{34} & F_{44} \end{pmatrix} \mathbf{\Phi}_0. \quad (2)$$

For convenience, we divide all scattering-matrix elements (except $F_{11}(\theta)$ itself) by $F_{11}(\theta)$, i.e., we consider $F_{ij}(\theta)/F_{11}(\theta)$, with i, $j = 1$–4 except for $i = j = 1$. The values of $F_{11}(\theta)$ are normalized so that they are equal to 1 at $\theta = 30°$ (Volten et al., 2006). The function $F_{11}(\theta)$, normalized in this way, is proportional to the flux of the scattered light for unpolarized incident light and called the phase function or scattering function in this paper. Also, for unpolarized incident light, the ratio $-F_{12}(\theta)/F_{11}(\theta)$ is called the degree of linear polarization of the scattered light.

3. Experimental procedure

3.1. Experimental apparatus

A photograph of the IAA cosmic dust laboratory is presented in Fig. 1. The design of this instrument is based on the Dutch instrument developed in the group of Hovenier in Amsterdam by
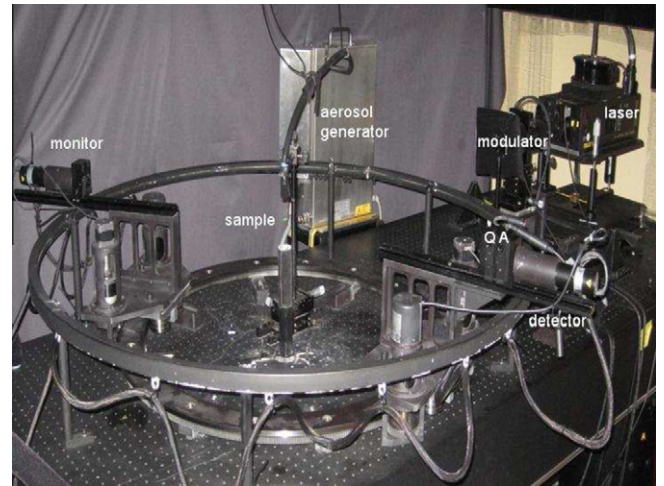
Fig. 1. Photograph of the experimental apparatus. On the right we can see the detector that moves along the ring. The ring is placed horizontally in the laboratory with an outer diameter of 1 m. The monitor is located on the left. In the middle, we see the nozzle of the aerosol generator located vertically in the center of the ring, and the green spot is where the laser beam interacts with the dust cloud. Q and A are the quarter-wave plate and analyzer, respectively. (For interpretation of the references to color in this figure legend, the reader is referred to the web version of this article.)

Stammes (1989) and Kuik (1992), and subsequently revised and significantly improved by Volten (2001) and Volten et al. (2001). Here we briefly summarize the main characteristics of the IAA apparatus. A detailed description of the instrument and reduction process is given by Muñoz et al. (2010).

Light from a linearly polarized continuous-wave tunable Argon–Krypton laser (483, 488, 520, 568, and 647 nm) passes through a polarizer and an electro-optic modulator. The modulated light is subsequently scattered by randomly oriented particles located in a jet stream produced by an aerosol generator. Thus, no vessel is needed to contain the sample at the point where the scattering takes place. This is a great advantage, since any object between the particles and the detector may cause e.g. reflections or stray light that decreases the accuracy of the measurements and limits the angular range. The particles of a particular mineral sample are brought into the jet stream as follows. A compacted amount of powder is loaded into a cylindrical reservoir. A piston pushes the powder onto a rotating brush at a certain speed. An air stream carries the aerosol particles of the brush through a tube to a nozzle above the scattering volume. In Fig. 2, we present a schematic picture of the aerosol generator. A filter wheel equipped with grey filters of different density is located between the laser and the polarizer. It is operated from the computer so that the flux of the incident beam can be scaled to its
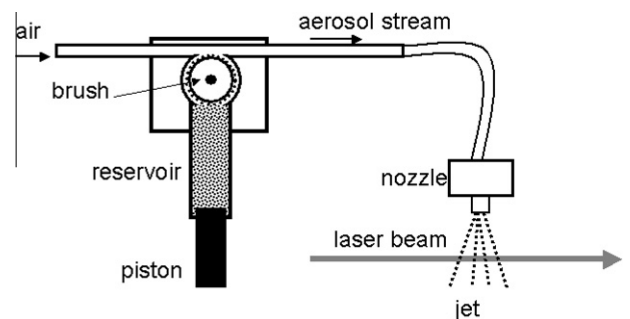
Fig. 2. Schematic picture of the aerosol generator. A piston in the cylindrical feed stock reservoir with a diameter of 10 mm pushes powder onto a rotating brush at a certain speed. An air stream carries the aerosol particles of the brush through a tube to a nozzle right above the scattering volume.

most appropriate value for each scattering angle. The scattered light passes through a quarter-wave plate, Q, and an analyzer, A, (both optional) and is detected by a photomultiplier tube, the detector. Another photomultiplier tube (the monitor) is located at a fixed position and is used to correct for fluctuations in the aerosol stream. By using eight different combinations for the orientation angles of the optical components, and assuming reciprocity of the sample (in particular $F_{21}/F_{11} = F_{12}/F_{11}$; $F_{31}/F_{11} = -F_{13}/F_{11}$; and $F_{41}/F_{11} = F_{14}/F_{11}$), all scattering-matrix elements are obtained as functions of the scattering angle (Hovenier, 2000).

The accuracy and reliability of the apparatus have been tested by comparing the measured scattering matrices of size-fitted water droplets at 488 nm, 520 nm, and 647 nm with Lorenz–Mie calculations for a distribution of homogeneous water droplets. As presented in Muñoz et al. (2010), the water droplets measurements showed an excellent agreement with the Lorenz–Mie computations over the entire angle range at the three studied wavelengths. Moreover, we always verify the reliability of the measurements by applying the Cloude coherency matrix test as suggested by Hovenier et al. (2004).

3.2. Single or multiple scattering

As mentioned in Section 2, the measurements of our experimental apparatus must be performed under single scattering conditions to fulfill Eqs. (1) and (2). Therefore, we must have enough particles in the scattering volume to be representative for the ensemble of randomly oriented particles under study but not so many that multiple scattering may start playing a role. To check if multiple scattering effects can be neglected in our experiments we performed a series of flux measurements with the detector in a fixed position as suggested by Hovenier et al. (2003). The speed of the piston that pushes the particles onto the rotating brush is then increased varying in this way the number of scattering particles. Since the number density of particles in the stream is proportional to the speed of the piston, the measured flux must increase linearly with the speed of the piston only under single scattering conditions, as the measured flux is proportional to the number density of particles in such conditions (see e.g. Van de Hulst, 1957; Kerker, 1969). In Fig. 3, we present the results of a multiple scattering test for a sample of white clay particles. The measurements were performed at 647 nm, fixing the detector at 10° scattering angle. Because small fluctuations in particle density in the continuous aerosol jet stream occur, we integrated the signals over relatively long periods of time to get reasonable accuracy. During a normal light scattering measurement with a dust sample, the piston speed must be high enough to obtain a stable aerosol stream but not too high to avoid an unnecessary waste of sample. Thus, the piston speed usually ranges from 40 to 100 mm/h depending on the sample under study. In this multiple scattering test the piston speed was varied from 50 mm/h to 250 mm/h in steps of 50 mm/h. As shown, even at speeds as high as 250 mm/h we do not find any significant deviation from a linear behavior, which means that multiple scattering effects can be neglected in our experiments.
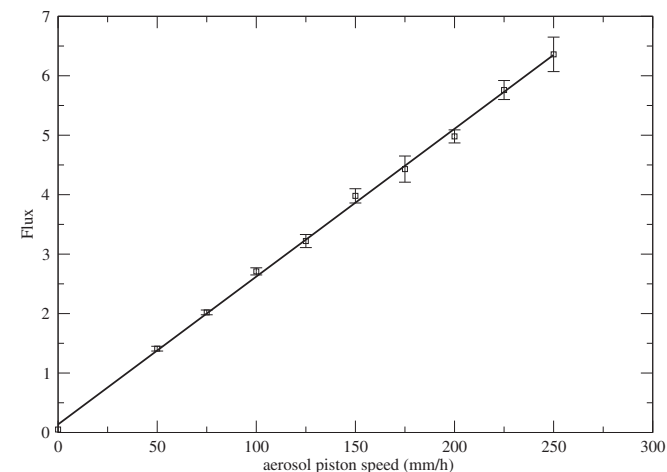
3.3. Particle aggregation

One of the most common questions about light scattering experiments is if the aerosol beam may change the shape/size of the particles, either by breaking them up in smaller particles or by aggregating them into larger particles. To test this, we perform Field Emission Scanning Electron Microscope (FESEM) images for the sample under study as it is during the light scattering measurements. A FESEM slide is used to collect particles directly in the jet stream by holding the slide briefly in the jet at the place where it intersects with the laser beam. A second FESEM slide is prepared with particles taken directly from the container.

In the upper panels of Fig. 4 we present FESEM images of some white clay particles directly collected from the aerosol jet (left panel) and from the container (right panel), at the same magnification. Comparison of the two images shows no evidence of a significant alteration of the particles due to the aerosol generator. In the bottom panel we present another FESEM image at a different magnification of the white clay particles collected from the aerosols jet.

3.4. Test sample

As mentioned in Section 3.1, the accuracy of the apparatus was tested by comparison of the measured scattering matrices for water droplets with results of Lorenz–Mie calculations for homogeneous spherical water droplets (Muñoz et al., 2010). As an extra test, we have performed measurements on a sample of green clay particles previously studied in the Amsterdam light scattering setup. For a detailed description of the physical properties of the green clay sample and the measured scattering matrix we refer to Muñoz et al. (2001). The measurements in Amsterdam were performed in 1999 at a wavelength of 632.8 nm. Ten years later, we have repeated the measurements with the same sample in the IAA cosmic dust laboratory. The measurements in Granada have been performed at a wavelength of 647 nm. In Fig. 5, we compare the measured scattering matrices in Amsterdam and Granada. Despite the fact the two scattering matrices have been measured so far away in time and with a different experimental apparatus in a different laboratory, the agreement in the measured results is really impressive. Within experimental errors each scattering-matrix element measured in Granada is on top of the same scattering matrix element measured in Amsterdam at nearly all measured scattering angles. The small deviations may at least partly be due to small differences in the wavelengths of the incident light and in some physical properties of the particles that could have changed over the years such as the size distribution and refractive index.

4. White clay measurements

4.1. Shapes and refractive index

Clay particles present a wide variety of irregular shapes. Fig. 4 shows Field Emission Scanning Electron Microscope (FESEM) of

Fig. 3. Flux of scattered light (in arbitrary units) versus aerosol generator speed for white clay particles. The detector is placed at a scattering angle of 10°. No indication of multiple scattering is found.
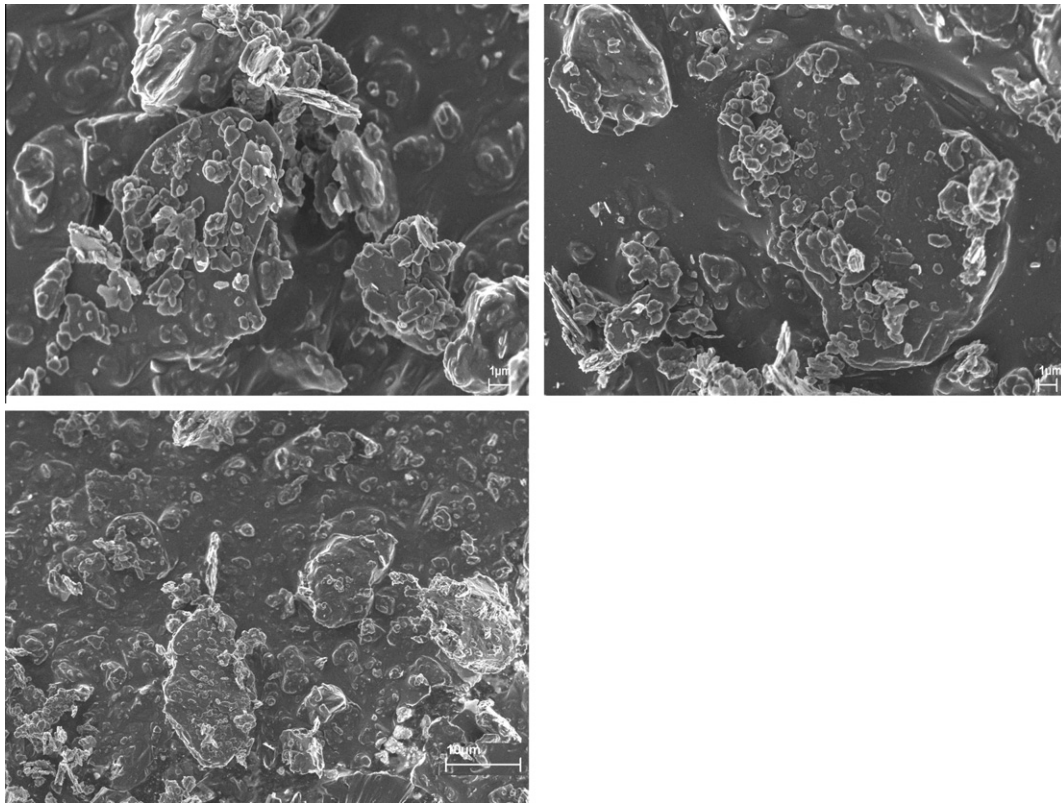
Fig. 4. FESEM images of white clay particles directly collected from the aerosol jet (top left and bottom panels) and collected from the container (top right panel).
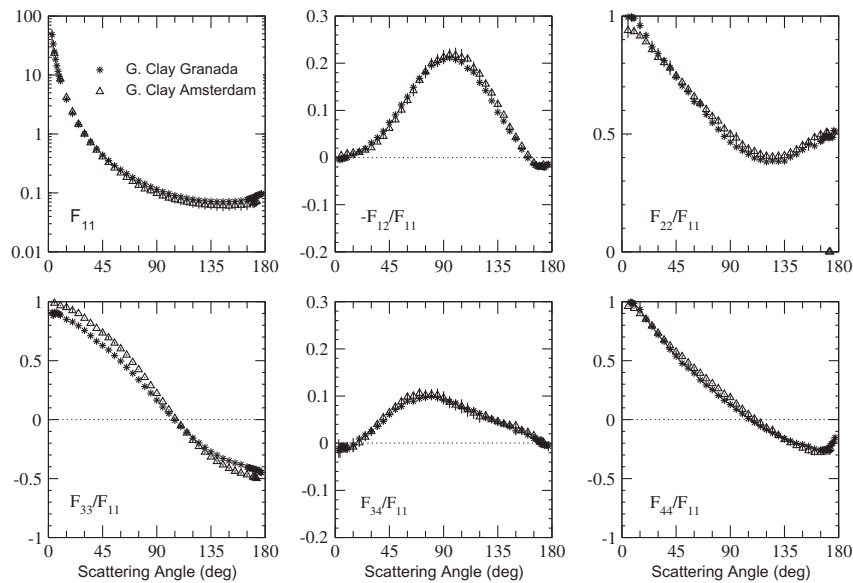
Fig. 5. Measured scattering matrices elements in Granada (stars) and Amsterdam (triangles) for a sample of green clay particles. Errors are presented by bars that sometimes are not seen because they are within the size of the symbols.

our sample of white clay particles. The particles in the sample present the typical sheet-like structure of clay particles.

The exact values of the refractive index of the white clay sample is unknown. Based on literature values (Kerr, 1959; Tröger et al., 1971; Egan and Hilgeman, 1979; Gerber and Hindman, 1982; Klein and Hurlbut, 1993), we can assume that the real part of the refractive index lies between 1.5 and 1.7, while the imaginary parts likely lies in the range between 10^{-2} and 10^{-5} at visual wavelengths. Because of the white color of this clay sample the

imaginary part of the refractive index is estimated to be in the neighborhood of 10^{-5}.

4.2. Size distributions

The great difficulty in getting accurate size distribution measurements for samples of irregular mineral particles is well known (see e.g. Reid et al., 2003). Most laser particle-sizing devices are based either on the Fraunhofer diffraction theory for spheres or

on the Lorenz–Mie theory. The Fraunhofer diffraction theory does not make assumptions about the refractive indices of the particles. However, it is only applicable to particles larger than the wavelength of the incident light. Lorenz–Mie theory provides exact results for any type of homogeneous spherical particles without any restriction about their sizes. In this case we need an estimation of the refractive index of the particles.

We use a Mastersizer 2000 from Malvern instruments to measure the volume distribution of our samples of irregular particles. The Mastersizer measures the phase function of the sample at 633 nm in a certain scattering angle range with special attention to the forward scattering peak. Once it is measured it uses either Lorenz–Mie theory or Fraunhofer theory for spheres to retrieve the volume distribution that best fits the measured scattering pattern. It is clear that the retrievals from both methods are simplifications based on the assumption that the particles of the sample under study are spherical. Moreover, the Fraunhofer method puts restrictions on the size of the particles. In the majority of the cases our samples of interest contain particles with irregular shapes distributed over broad size distributions with sizes ranging from sub-micron up to hundred microns. However, at this moment this is the best that can be done as far as particle sizing for broad distributions of irregular particles is concerned. Thus, we decided to present the volume distributions retrieved from both, Fraunhofer and Lorenz–Mie theory so that the reader can choose which one is more appropriate for her/his purposes or take the average. In general, increasing the size of a particle with a certain shape promotes diffraction and the shapes of diffraction peaks of collections of particles are similar for different shapes of the particles as confirmed by various computations (Mishchenko, 2009). Thus, results of both sizing methods tend to converge as the particles become larger. In Fig. 6, we plot the $V(\log r)$ as a function of $\log r$ for the sample of white clay particles. Here r is the radius of the volume-equivalent sphere of a particle. The $V(\log r)$ is obtained from the measured volume distribution, $v(r)$, as suggested in the Amsterdam Light Scattering Database http://www.astro.uva.nl/scatter (*an extensive explanation of the size distributions*) and in Volten et al. (2005). In this way, equal areas under parts of the curve mean equal relative volumes of particles per unit volume in the range considered. From the measured volume distributions we calculate the values of the effective radius, r_{eff}, and effective variance, v_{eff} as defined by Hansen and Travis (1974). The resulting values are presented in Table 1.
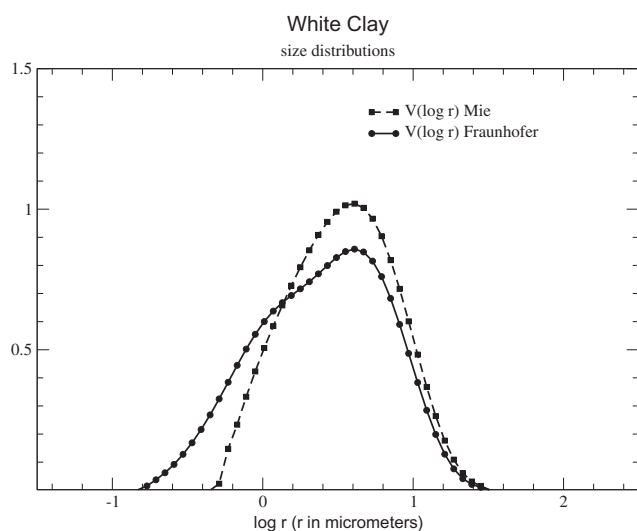
4.3. Measurements

In Fig. 7, we present all measured scattering-matrix elements as a function of the scattering angle of our sample of white clay particles. The measurements are performed at 647 nm. As mentioned, the measured phase functions are normalized to 1 at 30°. The other matrix elements are plotted relative to $F_{11}(\theta)$. As shown in Fig. 7, it is verified that in our experiments the scattering matrix has indeed the form given by Eq. (2), within experimental error. For that reason, we usually only plot the 8 elements that are not equal to zero for all scattering angles (cf. Figs. 5 and 8). In Fig. 8, we compare the measured scattering matrices at two different wavelengths, namely 488 and 647 nm. The scattering matrices fulfill the Cloude coherency matrix test within the experimental errors at all measured scattering angles (see e.g. Hovenier et al., 2004). The measured $F_{11}(\theta)$ presents a strong forward peak and almost no structure at side- and back-scattering angles. The degree of linear polarization for unpolarized incident light, $-F_{12}(\theta)/F_{11}(\theta)$, presents the typical bell-shape with a maximum around 90° and a negative branch at large scattering angles. The $F_{44}(\theta)/F_{11}(\theta)$ ratios are larger than the $F_{33}(\theta)/F_{11}(\theta)$ at scattering angles larger than about 100° whereas the $F_{22}(\theta)/F_{11}(\theta)$ is different from unity at nearly all measured scattering angles. In general the measured scattering-matrix elements as functions of the scattering angle present the typical behavior of irregular compact mineral particles with moderate refractive indices (see e.g. Volten et al., 2001, and the Amsterdam Light Scattering Database, http://www.astro.uva.nl/scatter).

When comparing the measurements at the two studied wavelengths we observe that the maximum of the degree of linear polarization increases when increasing the wavelength of the incident light. This wavelength dependence is probably due to the change in the apparent size of the particles i.e. the smaller the size parameter, the higher the maximum of the degree of linear polarization. Another possibility would be a strong wavelength dependence of the refractive index of the particles. However, that is highly unlikely for such a white sample. Moreover, the measured $F_{22}(\theta)/F_{11}(\theta)$ at 647 nm presents the highest values at almost all measured scattering angles. In contrast, the $F_{33}(\theta)/F_{11}(\theta)$, $F_{34}(\theta)/F_{11}(\theta)$, $F_{44}(\theta)/F_{11}(\theta)$ do not seem to show any significant wavelength dependence at the two studied wavelengths. Similar wavelength dependence was presented by previous measurements performed in Amsterdam with red and green clay particles and many other mineral particles (Volten et al., 2001; Muñoz et al., 2001, and http://www.astro.uva.nl/scatter).

5. Summary and outlook

We present the first scattering matrices for irregular dust particles obtained at the IAA cosmic dust laboratory. The reliability of the experimental apparatus has been tested by comparison of the measured scattering matrices for a sample of green clay particles with similar measurements previously performed at the Amsterdam light scattering setup. Moreover, we have checked that multiple scattering effects and changes in the sizes/shapes of the particles during the measurements are insignificant.

New measurements on a white clay sample are also presented. The measurements have been performed at 488 and 647 nm, in the

Fig. 6. Normalized volume distributions as a function of $\log r$ measured by a Mastersizer 2000 from Malvern instruments. The volume distributions have been retrieved by assuming Lorenz–Mie (dashed-squared line) and Fraunhofer (dashed-circled line) theories.

Table 1
Calculated effective radii, r_{eff}, and effective variances, v_{eff}, for the white clay sample.

Method	r_{eff} (μm)	v_{eff}
Fraunhofer	1.61	1.42
Lorenz–Mie	2.56	0.71
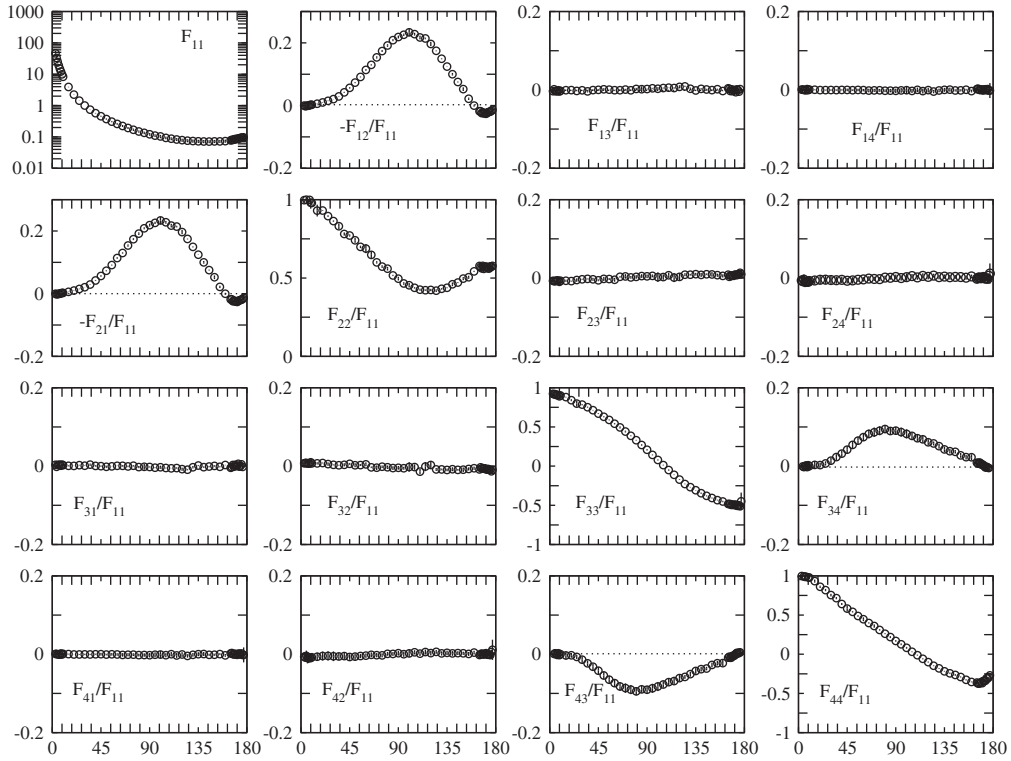
Fig. 7. All measured scattering-matrix elements for white clay particles at 647 nm. Errors are presented by bars that sometimes are not seen because they are within the size of the symbols.
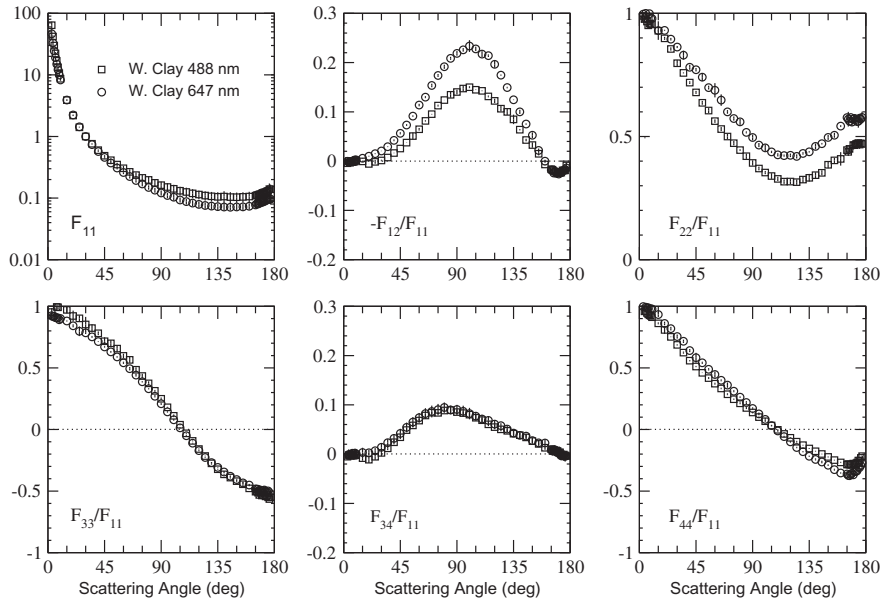
Fig. 8. Measured scattering matrices elements for a sample of white clay particles. The measurements are performed at 488 and 647 nm. Errors are presented by bars that sometimes are not seen because they are within the size of the symbols.

scattering angle ranges from 3° to 177°. The measured scattering-matrix elements present the typical behavior of irregular mineral particles (see e.g. Volten et al., 2001, and the Amsterdam Light Scattering Database, http://www.astro.uva.nl/scatter) showing the $F_{11}(\theta)$, $-F_{12}/F_{11}(\theta)$, and $F_{22}(\theta)/F_{11}(\theta)$ to have a clear wavelength dependence at almost all measured scattering angles. In contrast the $F_{22}/F_{11}(\theta)$, $F_{33}/F_{11}(\theta)$, and $F_{44}/F_{11}(\theta)$ ratios do not present any significant differences at the two studied wavelengths. The new white clay data will be included in tabular form in the new

Amsterdam–Granada Light Scattering Database at http://www.iaa.es/scattering, which is currently under construction.

The apparatus is devoted to experimentally studying the angle-dependent scattering matrices of dust samples of astrophysical interest. We are especially interested in mineral dust particles that are potential candidates for being present in the planetary and cometary atmospheres of the Solar System (e.g. olivines, pyroxenes, calcite, carbon, etc.). Moreover, there is great interest in measuring aerosol samples that can affect the radiative balance

of the Earth's atmosphere such as desert dust, volcanic ashes, and carbon soot.

Acknowledgments

References

Bandfield, J.L., 2002. Global mineral distributions on Mars. J. Geophys. Res., 107. doi:10.1029/2001JE001510.

Bland, P.A., Lee, M.R., Sexton, A.S., Franchi, I.A., Fallick, A.E.T., Miller, M.F., Cadogan, J.M., Berry, F.J., Pillinger, C.T., 2000. Aqueous alteration without a pronounced oxygen-isotopic shift: Implications for the asteroidal processing of chondritic materials. Meteorit. Planet. Sci. 35 (6), 1387–1395.

Clancy, R.T., Lee, S.W., Gladstone, G.R., McMillan, W.W., Roush, T., 1995. A new model for Mars atmospheric dust base upon analysis of ultraviolet through infrared observations from Mariner 9, Viking, and Phobos. J. Geophys. Res. 100, 5251–5263.

d'Almeida, G.A., Koepke, P., Shettle, E.P., 1991. Atmospherical aerosols: Global climatology and radiative characteristics. A. Deepak, Hampton, VA.

Draine, B.T., Flatau, P.J., 2003. User guide for the Discrete Dipole Approximation Code DDSCAT 6.0. <http://arxiv.org/abs/astro-ph/0309069>.

Egan, W.G., Hilgeman, T.W., 1979. Optical Properties of Inhomogeneous Materials: Applications to Geology, Astronomy, Chemistry, and Engineering. Academic, San Diego, CA.

Fulle, M., 2004. Motion of cometary dust. In: Festou, M.C., Keller, H.U., Weaver, H.A. (Eds.), Comets, vol. II. University of Arizona Press, pp. 565–575.

Gerber, H.E., Hindman, E.E. (Eds.), 1982. Light absorption by aerosol particles. In: Technical Proceedings of the First International Workshop on Light Absorption by Aerosol Particles, Fort Collins, Col., 1980, Spectrum, Hampton, VA.

Hansen, J.E., Travis, L.D., 1974. Light scattering in planetary atmospheres. Space Sci. Rev. 16, 527–610.

Hovenier, J.W., 2000. Measuring scattering matrices of small particles at optical wavelengths. In: Mishchenko, M.I., Hovenier, J.W., Travis, L.D. (Eds.), Light Scattering by Nonspherical Particles. Academic, San Diego, CA, pp. 355–365.

Hovenier, J.W., Muñoz, O., 2009. Light scattering in the Solar System: An introductory review. J. Quant. Spectrosc. Radiat. Trans. 110 (14–16), 1280–1292.

Hovenier, J.W., Volten, H., Muñoz, O., van der Zande, W.J., Waters, L.B.F.M., 2003. Laboratory studies of scattering matrices for randomly oriented particles. Potentials, problems, and perspectives. J. Quant. Spectrosc. Radiat. Trans., 741–755.

Hovenier, J.W., van der Mee, C.V.M., Domke, H., 2004. Transfer of polarized light in planetary atmospheres: Basic concepts and practical methods. Kluwer, Springer, Dordrecht, Berlin.

Kahnert, F.M., 2003. Numerical methods in electromagnetic scattering theory. J. Quant. Spectrosc. Radiat. Trans. 79, 775–824.

Kerker, M., 1969. The Scattering of Light and Other Electromagnetic Radiation. Academic Press, New York. p. 313.

Kerr, P.F., 1959. Optical Mineralogy. McGraw-Hill, New York.

Klein, C., Hurlbut Jr., C.S., 1993. Manual of Mineralogy. John Wiley, New York.

Kuik, F., 1992. Single Scattering by Ensembles of Particles with Various Shapes. Ph.D. Dissertation, Free University, Amsterdam.

Matsuki, A., Schwarzenboeck, A., Venzac, H., Laj, P., Crumeyrolle, S., Gomes, L., 2010. Cloud processing of mineral dust: Direct comparison of cloud residual and clear sky particles during AMMA aircraft campaign in summer. Atmos. Chem. Phys. 10 (3), 1057–1069.

Min, M., Hovenier, J.W., de Koter, A., 2005. Modeling optical properties of cosmic dust grains using a distribution of hollow spheres. Astron. Astrophys. 432 (3), 909–920.

Mishchenko, M.I., 2009. Electromagnetic scattering by nonspherical particles: A tutorial review. J. Quant. Spectrosc. Radiat. Trans. 110 (11), 808–832.

Mishchenko, M.I., Travis, L.D., Mackowski, D.W., 1996. T-matrix computations of light scattering by nonspherical particles: A review. J. Quant. Spectrosc. Radiat. Trans. 55, 535–575.

Mishchenko, M.I., Travis, L.D., Kahn, R.A., West, R.A., 1997. Modeling phase functions for dustlike tropospheric aerosols using a shape mixture of randomly oriented polydisperse spheroids. J. Geophys. Res. 102, 16831–16846.

Mishchenko, M.I., Hovenier, J.W., Travis, L.D., 2000. Light Scattering by Non spherical Particles: Theory, Measurements, and Applications. Academic Press, San Diego.

Moreno, F., Muñoz, O., Guirado, D., Vilaplana, R., 2007. Comet dust as a size distribution of irregularly shaped compact particles. J. Quant. Spectrosc. Radiat. Trans. 106, 348–359.

Muinonen, K., Nousiainen, T., Lindqvist, A., Muñoz, O., Videen, G., 2009. Light scattering by Gaussian particles with internal inclusions and roughened surfaces using ray optics. J. Quant. Spectrosc. Radiat. Trans. 110 (14–16), 1628–1639.

Muñoz, O., Moreno, F., Molina, A., Ortiz, J.L., 1999. A comparison of the structure of the aerosol layers in the great red SPOT of Jupiter and its surroundings before and after the 1993 SEB disturbance. Astron. Astrophys. 344, 355–361.

Muñoz, O., Volten, H., de Haan, J.F., Vassen, W., Hovenier, J.W., 2001. Experimental determination of scattering matrices of randomly oriented fly ash and clay particles at 442 and 633 nm. J. Geophys. Res. 106, 22833–22844.

Muñoz, O., Moreno, F., Guirado, D., Ramos, J.L., López, A., Girela, F., Jerónimo, J.M., Costillo, L.P., Bustamante, I., 2010. The new IAA light scattering apparatus. J. Quant. Spectrosc. Radiat. Trans. 111, 187–196.

Nousiainen, T., 2009. Optical modeling of mineral dust particles: A review. J. Quant. Spectrosc. Radiat. Trans. 110 (14–16), 1261–1279.

Nousiainen, T., Kahnert, M., Veihelmann, B., 2006. Light scattering modeling of small feldspar aerosol particles using polyhedral prisms and spheroids. J. Quant. Spectrosc. Radiat. Trans. 101 (3), 471–487.

Reid, J.S. et al., 2003. Comparison of size and morphological measurements of coarse mode dust particles from Africa. J. Geophys. Res., 108. doi:10.1029/2002JD002485.

Sokolik, I., Toon, O.B., 1999. Incorporation of mineralogical composition into models of the radiative properties of mineral aerosol from UV to IR wavelengths. J. Geophys. Res. 104 (D8), 9423–9444.

Stammes, P., 1989. Light Scattering Properties of Aerosols and the Radiation Inside a Planetary Atmosphere. Ph.D. Dissertation, Free University, Amsterdam.

Starukhina, L.V., Shkuratov, Yu.G., 1997. Surface composition of phobos. Solar Syst. Res. 31 (5), 381–386.

Taflove, A., Hagness, S.V., 2005. Advances in Computational Electrodynamics: The Finite-Difference Time–Domain Method, third ed. Artech House, Boston.

Tröger, W.E., Bambauer, H.U., Taborskky, F., Trochim, H.D., 1971. Optische Bestimmung der gesteinsbildenden Minerale Tl I: Bestimmungstabellen. Schweizerbart, Stuttgart, Germany.

Van de Hulst, H.C., 1957. Light Scattering by Small Particles. John Wiley, New York.

Vilaplana, R., Moreno, F., Molina, A., 2004. Computations of the single scattering properties of an ensemble of compact and inhomogeneous rectangular prisms: Implications for cometary dust. J. Quant. Spectrosc. Radiat. Trans. 88, 219–231.

Volten, H., 2001. Light Scattering by Small Planetary Particles. An Experimental Study. Ph.D. Dissertation, Free University, Amsterdam.

Volten, H., Muñoz, O., Rol, E., de Haan, J.F., Vassen, V., Hovenier, J.W., Muinonen, K., Nousianen, T., 2001. Scattering matrices of mineral aerosol particles at 441.6 nm and 632.8 nm. J. Geophys. Res. 106, 17375–17401.

Volten, H., Muñoz, O., Hovenier, J.W., de Haan, J.F., Vassen, W., van der Zande, W.J., Waters, L.B.F.M., 2005. WWW scattering matrix database for small mineral particles at 441.6 and 632.8 nm. J. Quant. Spectrosc. Radiat. Trans. 90 (2), 191–206.

Volten, H., Muñoz, O., Hovenier, J.W., 2006. Waters LBFM. An update of the Amsterdam light scattering database. J. Quant. Spectrosc. Radiat. Trans. 100, 437–443.

Webster, W.J., Johnston, K.J., Hobbs, R.W., Lamphear, E.S., Wade, C.M., Lowman, P.D., Kaplan, G.H., Seidelmann, P.K., 1988. The microwave spectrum of Asteroid Ceres. Astron. J. 95, 1263–1268.

Wolff, M.J. et al., 2006. Constraints on dust aerosols from the Mars Exploration Rovers using MGS overflights and Mini-TES. J. Geophys. Res. 111 (E12). CiteID E12S17.

Wriedt, T., 2009. Light scattering theories and computer codes. J. Quant. Spectrosc. Radiat. Trans. 110 (11), 833–843.

Yurkin, M.A., Hoekstra, A.G., 2007. The discrete dipole approximation: An overview and recent developments. J. Quant. Spectrosc. Radiat. Trans. 106, 558–589.

Zubko, E., Kimura, H., Shkuratov, Y., Muinonen, K., Yamamoto, T., Okamoto, H., Videen, G., 2009. Effect of absorption on light scattering by agglomerated debris particles. J. Quant. Spectrosc. Radiat. Trans. 110, 1741–1749.